Atom probe tomography-assisted kinetic assessment of spinodal decomposition in an Al-12.5 at.%Zn alloy

Xinren Chen, Xuyang Zhou, Frédéric de Geuser, Alisson Kwiatkowski da Silva, Huan Zhao, Eric Woods, Chuanlai Liu, Dirk Ponge, Baptiste Gault, Dierk Raabe

Atom probe tomography-assisted kinetic assessment of spinodal decomposition in an Al-12.5 at.%Zn alloy

Xinren Chen[a,*], Xuyang Zhou[a], Frédéric De Geuser[b], Alisson Kwiatkowski da Silva[a], Huan Zhao[a], Eric Woods[a], Chuanlai Liu[a,**], Dirk Ponge[a], Baptiste Gault[a,c], Dierk Raabe[a,***]

[a]*Max-Planck-Institut für Eisenforschung, Düsseldorf 40237, Germany*

[b]*University Grenoble Alpes, CNRS, Grenoble INP, SIMaP, Grenoble F-38000, France*

[c]*Department of Materials, Royal School of Mines, Imperial College, Prince Consort Road, London SW7 2BP, UK*

Abstract

The rates of atomic clustering and precipitation hardening are closely related to the diffusivity of solutes and the concentration of vacancies during the natural aging of aluminum alloys. Measuring the diffusivity of solutes at room temperature, especially in systems with an equilibrium vacancy concentration, benefits the design of the aging process. However, this measurement has long been challenging due to the extremely low diffusion rates of solutes in aluminum at room temperature and the presence of supersaturated vacancies. In this work, we propose a method to quantify the diffusivity of solutes based on the kinetic evaluation of the spinodal decomposition process. This evaluation involves conducting atom probe tomography experiments, analyzing the radial distribution function, and modeling the phase separation process using the Cahn-Hilliard theory. The aging experiments were conducted on nanoscale samples, where excess vacancies can be eliminated at free surfaces due to a high surface-to-volume ratio. The results yielded a diffusivity of Zn in the Al-12.5 at.% Zn alloy of $(1.32 \pm 0.46) \times 10^{-25}$ m²/s at 295 K. This work introduces a novel approach to assess solute diffusivity under conditions of equilibrium vacancy concentration at room temperature and expands the temperature range for measuring diffusivity in systems with spinodal decomposition, particularly in cases where kinetic data at low temperatures are scarce.

Keywords: Al-Zn alloy, diffusivity, atom probe tomography, spinodal decomposition, radial distribution function, nano aging

*Corresponding author

**Corresponding author

***Corresponding author

Email addresses: x.chen@mpie.de (Xinren Chen), c.liu@mpie.de (Chuanlai Liu), d.raabe@mpie.de (Dierk Raabe)

1. Introduction

Aluminum alloys are an important material group with the highest market growth rates in the electrified transportation sector. Age hardening aluminum alloys (2xxx, 6xxx, and 7xxx) can show a yield strength enhancement of up to half an order of magnitude compared to their annealed state after undergoing precipitation during aging [1]. The formation of precipitates, whether resulting from spinodal decomposition [2] or nucleation and growth [3], requires the diffusion of solutes.

The most effective strengthening can usually be achieved when precipitates are produced in very high dispersion, i.e., with very small sizes for a given precipitate volume fraction. Therefore, low-temperature heat treatment and aging are particularly important for the age hardening of aluminum alloys because they limit the diffusion length, resulting in smaller particles. For commercial 7xxx Al-Zn-based alloys, the diffusivity of Zn is important to determine the nucleation and growth rates of clusters [4], Guinier-Preston (GP) zones [5, 6] and precipitates [7, 8, 9]. Furthermore, the diffusivity of Zn is highly influenced by remaining excess vacancies from quenching or deformation [10, 11, 12]. Thus, the age hardening efficiency and the resulting mechanical and functional properties are sensitive to vacancy concentration.

The diffusivity of Zn in Al was investigated using conventional methods, including the diffusion couple method (DCM) [13, 14], across different temperature ranges (Table 1). However, the diffusivity of Zn in Al in a system with an equilibrium vacancy concentration at moderate temperatures below 383 K (the lowest temperature in Table 1) [1] remains elusive since the diffusion length of Zn atoms reduces to only a few nanometers over a typical measurement period (months), which is difficult to measure. Such diffusivity data are important for common service scenarios of commercial 7xxx aluminum alloys, including aging processes [15, 16, 17, 18], deformation behavior [19], and corrosion [20]. Additionally, understanding the diffusivity of Zn in Al alloys with an equilibrium vacancy concentration is a crucial reference for studying the oversaturation of vacancies. Due to the lack of experimental data, diffusivity at 295 K is usually calculated by extrapolating the high-temperature diffusivity data using the Arrhenius equation [21, 22]. However, the difference between the highest and lowest predicted Zn diffusivity data at 295 K shown in Table 2 is about three orders of magnitude, which implies that the diffusivity data at 295 K should be further validated by experiments.

The quantification of the kinetics of spinodal decomposition, as proposed in [10, 11, 23, 24], provides an alternative method for studying the diffusivity of solutes. Spinodal decomposition is characterized by the absence of a nucleation barrier [10, 23]. A key advantage of

[1] Rundman [10] and Rodolfo [11] studied the diffusivity of Zn in Al at 338 K and 228 K, respectively, by analyzing spinodal decomposition. They discussed their findings with respect to the influence of quenched-in vacancies, a scenario that results in an excess number of vacancies and leads to faster diffusion.

this method is that it involves local uphill diffusion with only nanoscale diffusion lengths to produce compositional fluctuation [25]. Furthermore, the use of atom probe tomography (APT) [26] has enabled high-resolution three-dimensional composition measurement, facilitating precise quantitative evaluation of compositional fluctuations [27].

In addition, conducting aging experiments on nanosized APT samples can be a valuable approach for mitigating the influence of non-equilibrium vacancies [28, 29]. Nanosized samples are particularly advantageous in this context due to their rapid loss of non-equilibrium vacancies, owing to their high surface-to-volume ratio. Henceforth, we will refer to the aging process conducted on nanoscale samples as the 'nano aging process' [28]. This study employs such a nano aging process to determine the diffusivity of Zn in an Al-12.5 at.% Zn alloy undergoing spinodal decomposition at 295 K [30]. Analyzing nanoscale compositional fluctuations during the spinodal decomposition process enables a quicker determination of diffusivity compared to traditional diffusion length analysis [13, 31].

Table 1: The temperature ranges (K) of the experiments performed to measure the impurity diffusion coefficient of Zn in face-centered cubic aluminum (fcc-Al).

Fricke [32]	Beerwald [33]	Hilliard [31]	Ceresara [34]	Fujikawa [35]	Beke [36]	Nicholls [37]	Fontell [38]
573–773	688–828	678–927	676–832	438–918	614–890	383–433	443, 473

Table 2: Predicted impurity diffusion coefficients of Zn in fcc-Al at 295 K calculated using the Arrhenius equation, employing diffusion activation energy obtained from different sources (m^2/s).

Fricke [32]	Beerwald [33]	Hilliard [31]	Ceresara [34]	Fujikawa [35]	Beke [36]	Nicholls [37]	Cui [39]
6.5×10^{-25}	3.0×10^{-24}	1.4×10^{-27}	2.6×10^{-27}	2.2×10^{-26}	3.5×10^{-26}	3.4×10^{-26}	1.2×10^{-24}

2. Experimental methods

2.1. Materials and heat treatments

The Al-12.5 at.%Zn alloy (Table 3) was first synthesized in a vacuum induction furnace and cast as rectangular ingots (the segregated edges of the slab were cut off). The cast ingots were hot-rolled at 673 K and homogenized at 673 K. The samples were solutionized at 793 K for 2 hours and quenched to 295 K before sample grinding, polishing, and plasma-focused ion beam (PFIB) milling. Following PFIB milling, the samples were processed into nanosized needle specimens. After being sharpened, these needle specimens were placed in a vacuum for over one day to eliminate excess vacancies inherited from quenching or potentially from PFIB milling.

Table 3: Final bulk composition analysis of the target alloy by energy dispersive spectrometry (at.%).

Al	Zn	Fe	Si	Cu
Balance	12.5±0.6	<0.2	<0.1	<0.1

2.2. APT experiments

The APT data acquisitions were performed on a Cameca Instrument Inc. Local Electrode Atom Probe (LEAP) 5000XS. Samples were run in a voltage mode with a pulse fraction of 15%, a frequency of 200 kHz, and a detection rate of 0.5% at a temperature of 50 K. Reconstruction and analysis were performed using the commercial programme IVAS in AP Suite 6.1. The reconstruction parameters - field factor K_f and image compression factor - were calibrated according to the observed angles between the selected poles and the crystalline interplanar distance of these selected poles [40] (see Supplementary Note 1).

2.3. Nano aging experiments

The dimensions of an APT specimen are usually between 20 nm and 150 nm (Fig. 1a), thus excess vacancies can easily diffuse to the free surface of the specimen and be eliminated/annihilated [28]. Therefore, the vacancy concentration in nanoscale APT needle specimens usually decreases to the equilibrium concentration after a few seconds or minutes [28, 29]. As mentioned earlier, the aging processes of nanosized specimens are referred to as nano aging in this work.

The initial state of nano aging is notably affected by quenched-in vacancies before undergoing the process of sharpening to a nano size. Consequently, variations in bulk aging time, even for minutes following quenching, result in different initial sample conditions [41], making it challenging to obtain samples with the same initial state. The impact of these quenched-in vacancies will be elucidated in a separate study. To obtain more nano aging results for diffusivity analysis, the experiments were repeated four times (labeled as #1-#4 in Table 4), and the sample state determined by the first APT data acquisition in each of the experiments is defined as the initial state for each of the experiments. After nano aging at 295 (±1) K for a specified time (see Table 4), the specimens were subjected to APT experiments again to obtain the atomic distribution after nano aging, as shown in Fig. 1 a-c.

Table 4: Aging time for four nano aging experiments (aged at 295 K).

Experiment number	#1	#2	#3	#4
Nano aging time (hour)	600	840	1098	1098

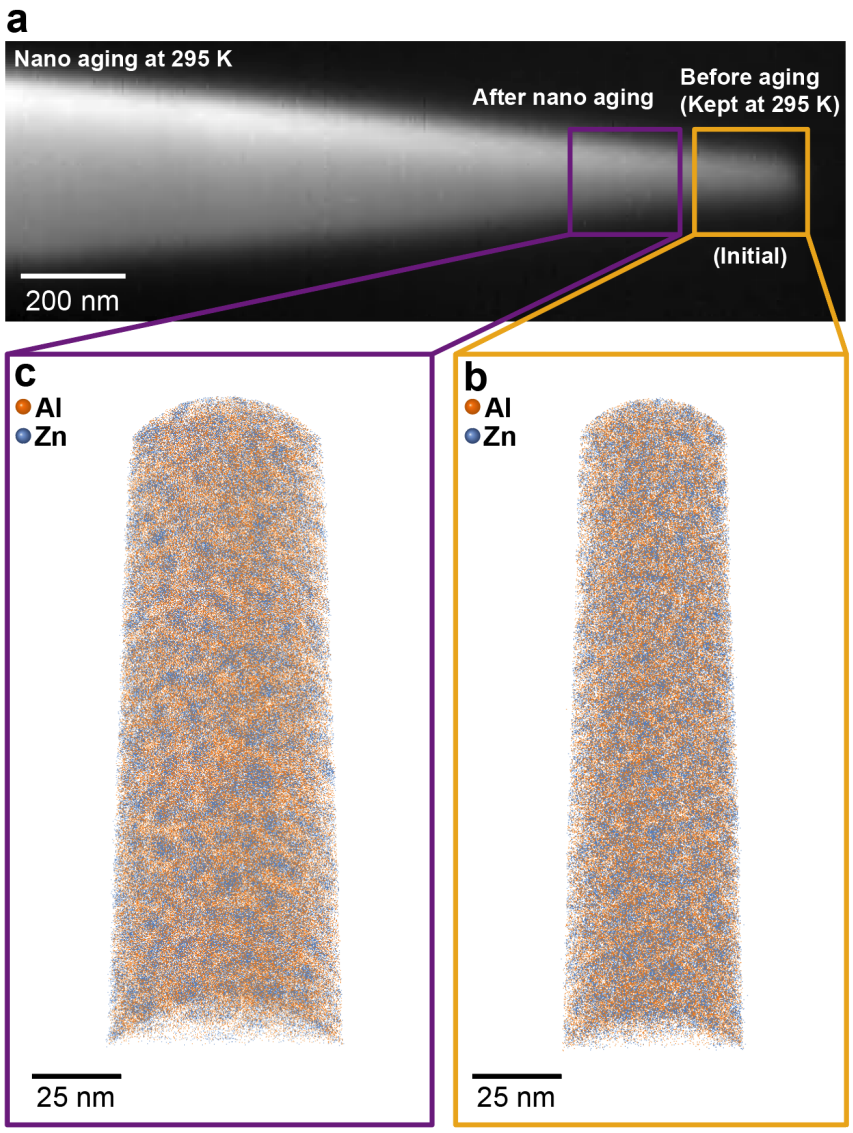

Figure 1: Illustration of the nano aging experiments: a. Scanning electron microscopy image of the APT needle specimen from Experiment #4 (see Table 4) before undergoing nano aging. b. Atomic distribution of the initial state of Experiment #4 (see Table 4). c. Atomic distribution after nano aging for 1098 hours at 295 K of Experiment #4 (see Table 4).

2.4. Small-angle X-ray scattering experiments

Small-angle X-ray scattering (SAXS) experiments were performed on a custom-built SAXS bench at SIMaP (France). The source is a rotating Cu anode producing 8.04 keV photons. The detector used was a Dectris Pilatus 2 located about 50 cm from the sample and kept under vacuum to minimize background. Data were background corrected and normalized based on incident intensity, sample transmission, and sample thickness using a calibrated PIN diode mounted in the beam stop and a glassy carbon sample used as a secondary calibration sample. Mechanical grinding was used to achieve a thickness of 70 to 100 μm. The sample for the SAXS was solutionized for 1 hour at 793 K, then quenched in water and immediately placed in the SAXS and recording started. The first measurement was taken 4 minutes after quenching.

3. Analysis methods

3.1. Radial distribution function analysis

The radial distribution function (RDF) calculates the probability function for finding target atoms at a radius of r to an origin center atom (see [42, 43, 44]). The bulk concentration normalized RDF can be expressed as:

$$\mathrm{RDF}(r) = \frac{c_{\mathrm{E}}(r)}{c_0} = \frac{N_{\mathrm{E}}(r)/N(r)}{c_0}, \tag{1}$$

where $c_{\mathrm{E}}(r)$ is the local atomic composition of targeted element E at the radius of r, c_0 the average bulk composition of element E in the analyzed volume, $N_{\mathrm{E}}(r)$ the total number of element E atoms from the radius of r to $r + dr$, and $N(r)$ the total number of all atoms in the shell region from the radius of r to $r + dr$. For the RDF results presented in this work, the step size dr is 0.2 nm.

The RDF value at radius 0 (RDF0) represents the theoretical possibility of finding the atoms of element E at the origin center location. If the origin and target elements are the same (e.g., in this case, both are Zn), the bulk concentration normalized RDF0 follows the relation [27]:

$$\mathrm{RDF0} = \frac{1}{V}\int\left(\frac{c_{\mathrm{E}}(x,y,z)}{c_0}\right)^2 dV. \tag{2}$$

3.2. Methods for mobility measurement

3.2.1. Cahn's method [23]

The analyses of the kinetics of spinodal decomposition are based on the Cahn-Hilliard (CH) equation [23],

$$\frac{\partial c}{\partial t} = M\left(\frac{\partial^2 f_{\text{chem}}}{\partial c^2} + \frac{\partial^2 f_{\text{e}}}{\partial c^2}\right)\nabla^2 c - 2M\kappa\nabla^4 c, \tag{3}$$

where c is the composition and M is the mobility. f_{chem} and f_{e} are the chemical free energy and elastic energy per unit volume, respectively. The gradient energy coefficient is denoted by κ.

Replacing c in Eq. (3) by a sinusoidal fluctuation of $c - c_0 = A(\beta, t)\cos\beta x$ where β is the angular wavenumber (use the wavenumber corresponding to the maximum growth rate [23]), and c_0 is the initial composition, one can obtain,

$$\frac{\partial A}{\partial t} = -M\left(\frac{\partial^2 f_{\text{chem}}}{\partial c^2} + \frac{\partial^2 f_{\text{e}}}{\partial c^2}\right)\beta^2 A - 2M\kappa\beta^4 A. \tag{4}$$

For a situation of infinitesimal fluctuation, the above equation has a solution:

$$A(\beta, t) = A(\beta, 0)\exp(R(\boldsymbol{\beta})t), \tag{5}$$

where

$$R(\boldsymbol{\beta}) = -M\beta^2\left(\frac{\partial^2 f_{\text{chem}}}{\partial c^2} + \frac{\partial^2 f_{\text{e}}}{\partial c^2} + 2\beta^2\kappa\right). \tag{6}$$

Thus, the mobility can be evaluated by,

$$M = \ln\left(\frac{A(\beta, t)}{A(\beta, 0)}\right) / \left[-\beta^2\left(\frac{\partial^2 f_{\text{chem}}}{\partial c^2} + \frac{\partial^2 f_{\text{e}}}{\partial c^2} + 2\beta^2\kappa\right)\Delta t\right]. \tag{7}$$

Eq. (7) is used only for the early stages of spinodal decomposition with infinitesimal fluctuations (due to the approximation of infinitesimal sinusoidal fluctuations to obtain an analytic solution [23]). However, after quenching, the spinodal decomposition can evolve very rapidly due to the excess vacancies from quenching [41], so that the initial state already deviates from the infinitesimal fluctuation situation. The time integration of the numerical solution in the following subsection of the Cahn-Hilliard equation (Eq. (3)) gives a more accurate simulation of the composition field than using Eq. (5). In this way, the method can be better adapted to the use for extended time scales for performing nano aging and APT analysis.

3.2.2. The numerical solution of the Cahn-Hilliard equation

For a homogeneous solution, the system incorporates fluctuation components with continuous wavelengths, which can be expressed by [23],

$$c(\boldsymbol{r}, t) = c_0 + \int_{\boldsymbol{\beta}} A(\boldsymbol{\beta}, 0)\exp(i\boldsymbol{\beta}\cdot r)d\boldsymbol{\beta}. \tag{8}$$

Eq. (8) can be expressed as a Fourier series by performing a Fourier transform [45]. For calculating the evolution of compositional fluctuations, the Cahn-Hilliard equation (Eq. (3)) was performed as follows:

$$\frac{\partial\{c\}_k}{\partial t} = -k^2 M\left[\left\{\frac{\Delta f_{\text{chem}}}{\Delta c}\right\}_k + \left\{\frac{\Delta f_{\text{e}}}{\Delta c}\right\}_k + 2k^2\kappa\{c\}_k\right], \tag{9}$$

where $\{.\}_k$ is the Fourier transform of the quantity inside the bracket and k is the vector in Fourier space. By treating linear and fourth-order operators implicitly and the nonlinear terms explicitly, the equation can be solved in a semi-implicit form [46]:

$$\frac{\{c\}_k^{n+1} - \{c\}_k^n}{dt_{\text{Sim}}} = -k^2\left\{\frac{\Delta f_{\text{chem}}}{\Delta c}\right\}_k^n - k^2\left\{\frac{\partial f_{\text{e}}}{\Delta c}\right\}_k^n - 2k^4\kappa\{c\}_k^{n+1}, \tag{10}$$

where $dt_{\text{Sim}} = Mdt$.

The RDF0 is calculated from the composition fields in the datasets obtained from experiments and simulations that are based on Eq. (10), using Eq. (1) and Eq. (2), respectively. During the nano aging experiments, after an aging time Δt_{Exp}, the RDF0 of the target solute element changes from RDF0($t = 0$) to RDF0($t = \Delta t_{\text{Exp}}$). Then, the time steps in simulation (Δt_{Sim}) required for the system to evolve from RDF0($t = 0$) to RDF0($t = \Delta t_{\text{Exp}}$) can be determined accordingly.

Thus, M can be calculated using the following relation:

$$M = \frac{\Delta t_{\text{Sim}}}{\Delta t_{\text{Exp}}}. \tag{11}$$

3.2.3. Chemical and elastic energy

The CALPHAD-based chemical free energy in this work is given by,

$$\Omega f_{\text{chem}} = \sum_{i=1}^{M} c_i G_i^0 + RT\sum_{i=1}^{M}(c_i \ln c_i) + G_{\text{chem}}^{\text{xs}}, \tag{12}$$

where Ω is the molar volume, c_i the composition of the component i, and G_i^0 the molar Gibbs free energy for the pure elements in a specified lattice structure. T denotes the absolute temperature, and R is the ideal gas constant. $G_{\text{chem}}^{\text{xs}}$ expresses the non-ideal interactions between elements in the phase, and is modeled by the Redlich-Kister polynomial [47, 48].

According to the work [23], the local elastic strain energy per unit volume is :

$$f_{\text{e}} = \frac{E}{1-\nu}\left[\eta\left(c - c_0\right)\right]^2, \tag{13}$$

where η is the linear expansion per unit composition change (for Zn, $\eta_{\mathrm{Zn}} = 0.0257$ [23]). E is the Young's modulus (70 GPa in this case) for the average composition, and ν is Poisson's ratio.

3.2.4. Interfacial gradient coefficient

Based on the statistical mechanical derivation, Cahn and Hilliard [49] derived,

$$\kappa = \omega\psi^2/2, \tag{14}$$

where ω is an interaction energy and ψ is an interaction distance. For a regular solution,

$$\omega = 4h^M_{0.5}, \tag{15}$$

in which $h^M_{0.5}$ is the integral heat of mixing per unit volume at $c = 0.5$. Based on Eq. (14), κ was suggested between $1.8 \sim 8.5 \times 10^{-6}$ erg cm^{-1} for Al-Zn system [10].

For a more precise determination of κ, small-angle X-ray scattering experiments (SAXS) [10, 25] were performed as described in Section 2.4. Fig. 2 shows the SAXS results during the natural aging process of the Al-12.5 at.% Zn alloy, which was quenched from 793 K and subsequently aged at 295 K. The fluctuation components at a wave vector below a critical wave vector q_{c} decay during the subsequent aging [23]. The intersection of the SAXS curves in Fig. 2 represents the boundary between the decay and growth regions, suggesting that the value of q_{c} is 1.15 nm^{-1}. Subsequently, the value of the gradient energy coefficient κ was determined using the critical wave vector q_{c} and Eq. (16),

$$\kappa = \left[\left(\frac{\partial^2 f_{\mathrm{chem}}}{\partial c^2} + \frac{\partial^2 f_{\mathrm{e}}}{\partial c^2}\right)\right] / (-2{q_{\mathrm{c}}}^2). \tag{16}$$

4. Experimental results

4.1. APT results

Fig. 3 shows the atomic distribution in the dataset obtained from experiment #2 in Table 4 before nano aging (initial state) and after nano aging at 295 K for 35 days. In comparison, the distribution of Zn atoms changed after nano aging, as shown in Figs. 3a and b. The size of Zn-enriched regions, which are clearly visible in the aggregation of blue dots roughly shaped like a sphere, is larger ($\sim$ 4 nm) than in the initial state ($\sim$ 3 nm). This is illustrated in Figs. 3c and d by the superposition of a series of 18 at.%Zn isosurfaces (the 18 at.%Zn isosurfaces enclose the positive compositional fluctuation above 18 at.%Zn) that delineate larger Zn-enriched regions after nano aging.

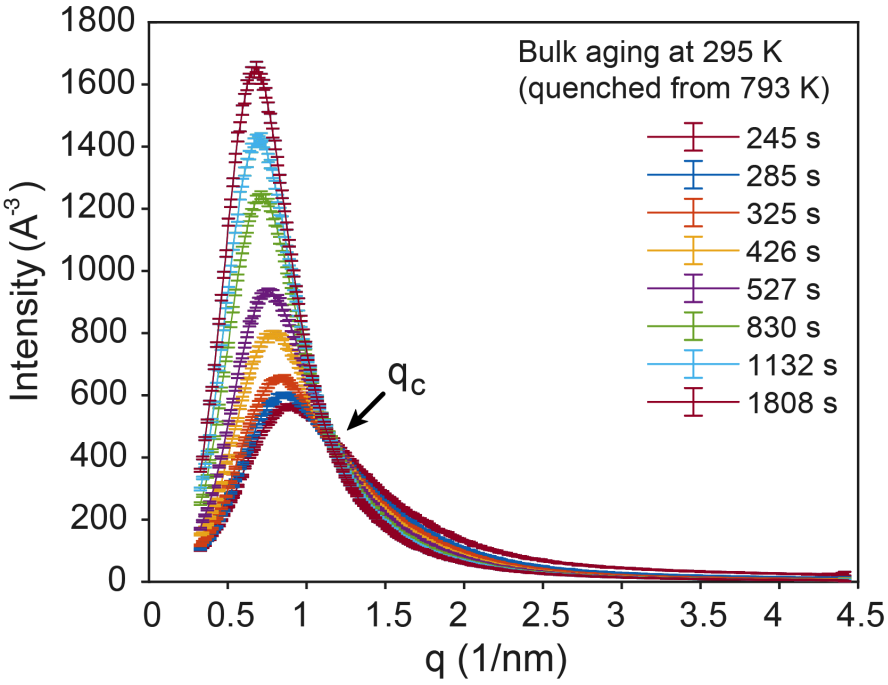

Figure 2: The results of small-angle X-ray scattering (SAXS) during the natural aging process of the Al-12.5 at.% Zn alloy, which was quenched from 793 K and subsequently aged at 295 K.

4.2. RDF results

Fig. 4 presents the Zn-Zn RDF results before and after performing nano aging of experiment #2 in Table 4. As mentioned in Section 3, the amplitude of compositional fluctuations can be quantified by RDF0. Fig. 4 shows an increase in RDF0 value from 1.68±0.05 to 1.94±0.11 after nano aging for 35 days. Similar results were obtained after nano aging of all samples at 295 K, and the respective increases are shown in Fig. 5 and Table 5 for comparison. The RDF0 increase over time are very close for experiments #2-#4 ($3.13 \sim 3.89 \times 10^{-4}$ hour^{-1}). For experiment #1 with a lower initial RDF0, the RDF0 rise rate is slightly lower than in the other experiments (1.92×10^{-4} hour^{-1}).

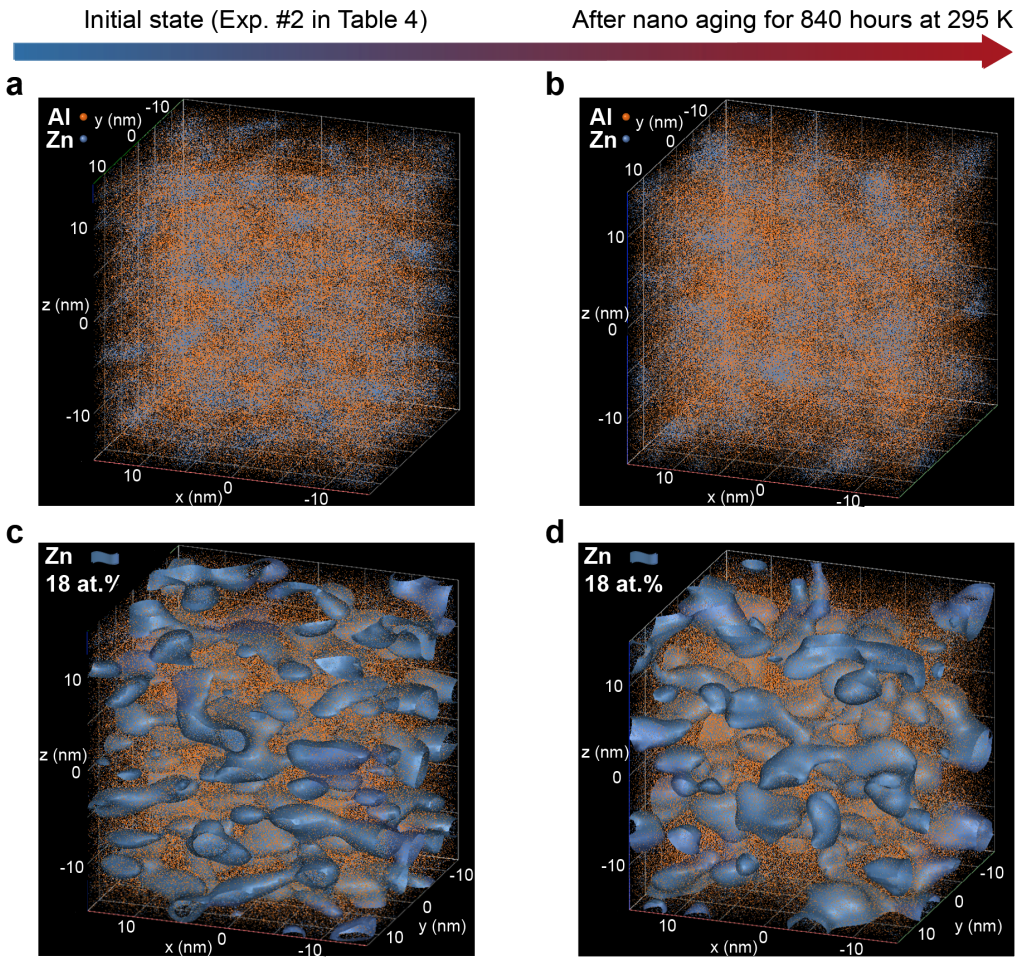

Figure 3: a. The initial atomic distribution in the dataset obtained from experiment #2 (see Table 4). b. The atomic distribution after nano aging for 840 hours at 295 K. c. Isosurfaces of 18 at.% Zn (5.5 at.% higher than the bulk Zn composition) from a. d. Isosurfaces of 18 at.% Zn from b.

Fig. 6 presents the simulation results of the composition fields c^{Sim} for the Al-12.5 at.%

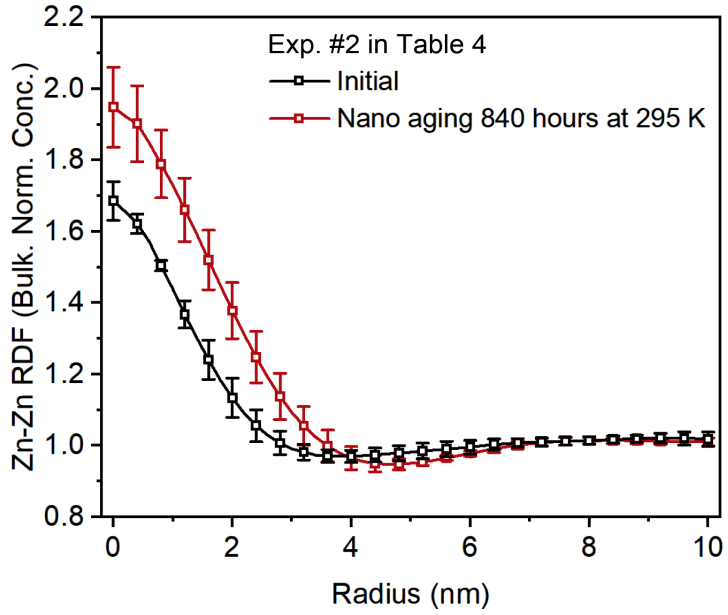

Figure 4: The Zn-Zn radial distribution function (RDF) results before and after nano aging of Experiment #2 (see Table 4). The RDF at radius 0 (RDF0) is obtained from the linear extension of the RDF at a radius of 0.2 nm to 0 nm.

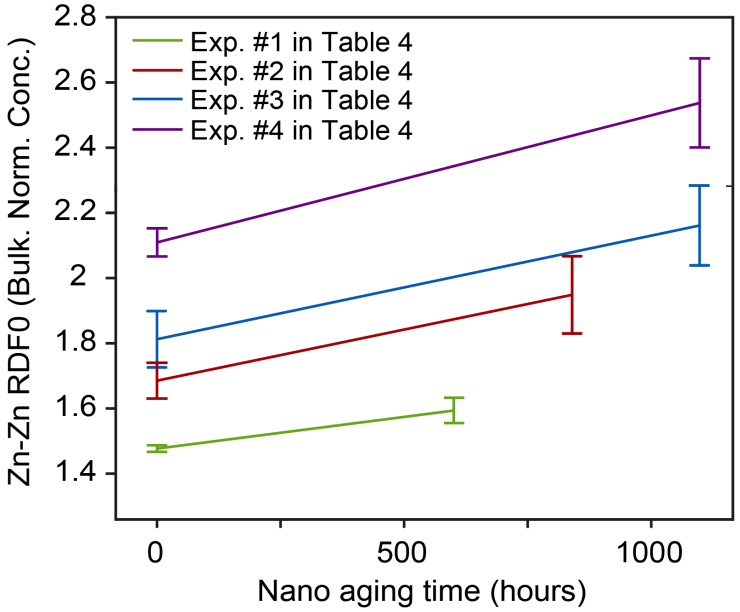

Figure 5: The experimental values of the Zn-Zn radial distribution function at radius 0 (RDF0) before and after nano aging from four nano aging experiments at 295 K (Experiment number #1-#4, see Table 4). The RDF0 is obtained from the linear extension of the RDF at a radius of 0.2 nm to 0 nm.

Table 5: The increase of RDF0 (hour^{-1}) during the four nano aging experiments in Table 4.

Exp. #1	Exp. #2	Exp. #3	Exp. #4
1.92×10^{-4}	3.13×10^{-4}	3.18×10^{-4}	3.89×10^{-4}

Zn alloy, obtained by solving Eq. (10). These simulated composition fields c^{Sim} were then utilized to compute the RDF0 through Eq. (2).

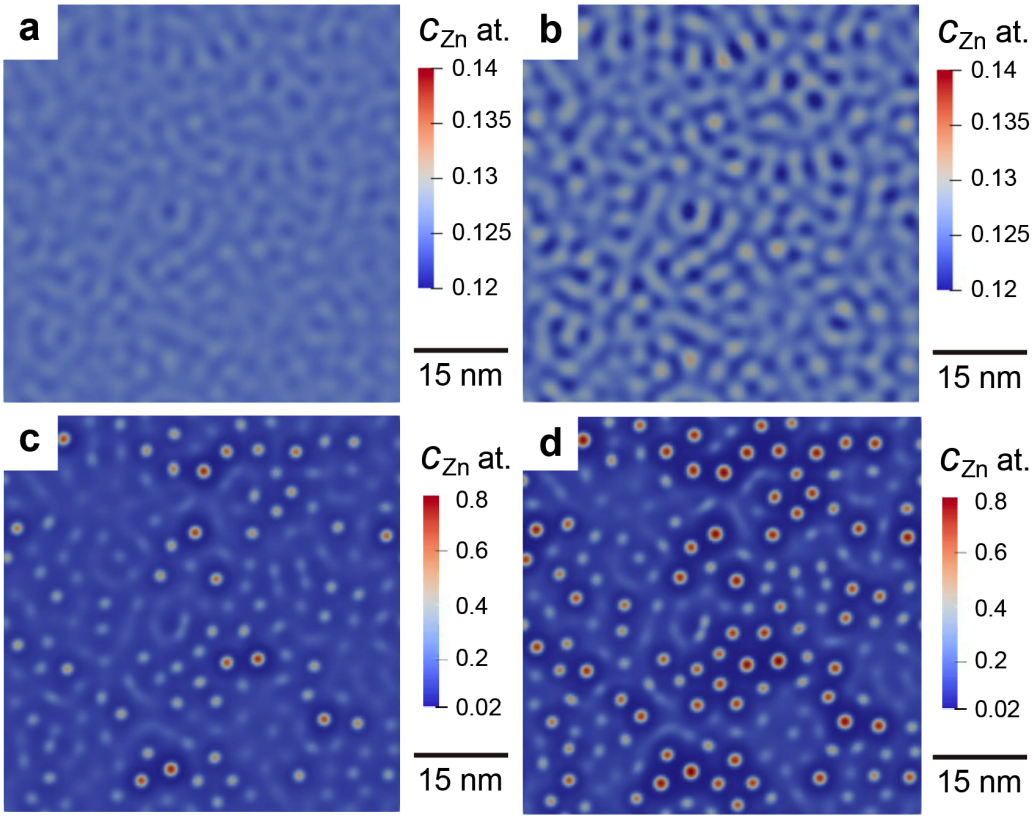

Figure 6: Zn composition field simulation during the spinodal decomposition of the Al-12.5 at.% Zn alloy. a. $t_{\text{Sim}} = 3.75 \times 10^{-22}$ m^5/J. b. $t_{\text{Sim}} = 5.63 \times 10^{-22}$ m^5/J. c. $t_{\text{Sim}} = 1.01 \times 10^{-21}$ m^5/J. d. $t_{\text{Sim}} = 1.07 \times 10^{-21}$ m^5/J.

The simulated RDF0 results are shown in Fig. 7. After a total simulation time of Δt_{Sim}, the RDF0 transitions from its initial state to the RDF0 after nano aging. Subsequently, Δt_{Sim} for each nano aging experiment was determined by using Fig. 7.

4.3. Diffusivity results

Using RDF0 data from four nano aging experiments (Fig. 5) and the corresponding Δt_{Sim} (Fig. 7) and Δt_{Exp}, the Zn mobility at 295 K in the Al-12.5 at.% Zn alloy can be estimated

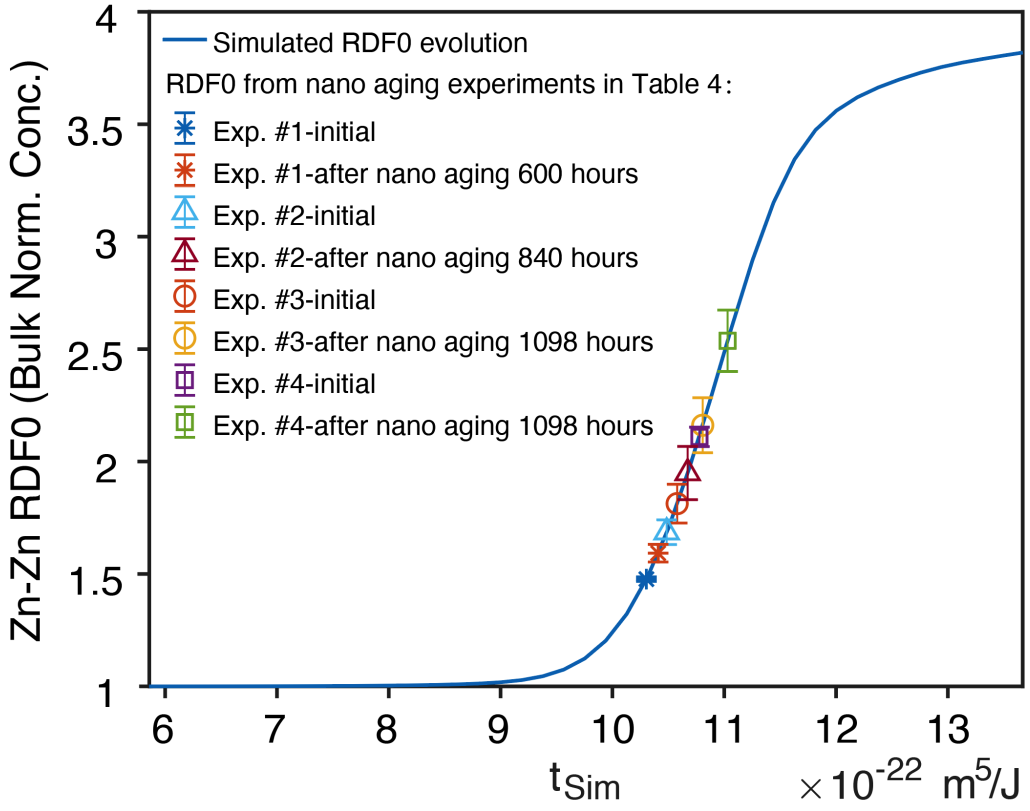

Figure 7: The simulated Zn-Zn radial distribution function at radius 0 (RDF0) from the simulation of the spinodal decomposition of the Al-12.5 at.%Zn alloy at 295 K and the RDF0 data points obtained from the nano aging experiments of the Al-12.5 at.%Zn alloy at 295 K. The experimental RDF0 is obtained from the linear extension of the RDF at a radius of 0.2 nm to 0 nm.

using Eq. (11) as mentioned in Section 3.2. The interdiffusion coefficient is related to the mobility through

$$\widetilde{D} = M\left(\frac{\partial^2 f_{\text{chem}}}{\partial c^2} + \frac{\partial^2 f_{\text{e}}}{\partial c^2}\right). \tag{17}$$

The results of the interdiffusion coefficient of Zn in the Al-12.5 at.%Zn alloy are shown in Table 6. Four nano aging experiments give an average interdiffusion coefficient of $(-2.78 \pm 0.97) \times 10^{-26}$ m^2 s^{-1}.

Table 6: Interdiffusion coefficients of Zn in the Al-12.5 at.% Zn alloy at 295 K ($\times 10^{-26} \pm 10^{-26}$ m^2/s) from four nano aging experiments in Table 4.

Exp. #1	Exp. #2	Exp. #3	Exp. #4
-2.32 ± 0.66	-2.91 ± 1.19	-2.69 ± 1.03	-3.05 ± 0.92

The mobility M can be calculated from tracer coefficients [50] as follows:

$$M_{\text{Zn}}/\Omega = [c_{\text{Zn}}(1 - c_{\text{Zn}})/RT]\left[c_{\text{Zn}}D^*_{\text{Al}} + (1 - c_{\text{Zn}})D^*_{\text{Zn}}\right], \tag{18}$$

where D^*_{Al} and D^*_{Zn} are tracer diffusion coefficients of Al and Zn in fcc-Al.

The tracer diffusion coefficient is described by the Arrhenius equation [21, 22]:

$$D^* = D^*_0 \exp\left(\frac{-Q}{RT}\right), \tag{19}$$

where D^*_0 is denoted as the pre-exponential factor and Q is the diffusion activation energy.

The Darken equation [51] that incorporates the thermodynamic factor, $\Phi = 1 + \frac{\partial \ln \gamma}{\partial \ln c}$ where γ is the activity coefficient, is used to correlate the interdiffusion coefficient to tracer diffusion coefficients, given as:

$$\widetilde{D} = \left[(1 - c_{\text{Zn}})D^*_{\text{Zn}} + c_{\text{Zn}}D^*_{\text{Al}}\right]\Phi. \tag{20}$$

In this work, $D^*_{\text{Zn}} \approx \widetilde{D}/\Phi$ was used to obtain the tracer diffusion coefficient of Zn in Al as $c_{\text{Zn}} < 0.2$, which equals the impurity diffusion coefficient [52] that represents the diffusivity of Zn in an extremely small Zn composition Al-Zn alloy.

The estimated Zn impurity diffusion coefficients in Al-Zn solid solutions at 295 K are given in Table 7.

Fig. 8 shows a comparison of Zn impurity diffusion coefficient data with Arrhenius law predictions. The four nano aging experiments on the Al-12.5 at.%Zn alloy yield an average impurity diffusivity of Zn in the Al-Zn solid solution of 1.32×10^{-25} m^2 s^{-1} with an error of $\pm 0.46 \times 10^{-25}$ m^2 s^{-1}, which is close to the majority of values predicted by the Arrhenius equation (Hilliard [31], Ceresara [34], Beke [36], Fujikawa [35], Nicholls [37]).

Table 7: The results of the impurity diffusion coefficient of Zn in the Al-Zn solid solution at 295 K ($\times 10^{-25} \pm 10^{-25}$ m^2/s).

Exp. #1	Exp. #2	Exp. #3	Exp. #4
1.10 ± 0.31	1.38 ± 0.57	1.28 ± 0.49	1.45 ± 0.44

5. Discussion

5.1. Error estimation

The statistical errors in Table 7 were determined by quantifying the deviation of the diffusivity calculated using RDF0 from the experimental measurements, as depicted in Fig. 5. The error in RDF0 is typically attributed to random compositional fluctuations [24], sampling location variations, and other common artefacts in composition measurements encountered in APT. [44].

It can be observed in Fig. 5 that the measurement error of RDF0 increases with higher RDF0 values. This occurs because, as the second phase grows, the number of second-phase particles within the selected region with the same volume used for calculating RDF0, decreases accordingly. To mitigate this, it is advisable to select more regions and compute their average RDF0 values to enhance the reliability of RDF0 measurements and to use APT specimens with larger top radii.

5.2. The effect of thermodynamic assessment

It should be pointed out that, according to Eqs. (7) and (9), the precision of the calculated mobility relies on the accuracy of the driving force for spinodal decomposition, which encompasses aspects of both thermodynamics and elasticity.

The thermodynamic driving force $\partial^2 f_{\text{chem}}/\partial c^2$ (as shown in Table 8) was estimated using Eq. (12) and parameters from Ref. [47], which extensively assesses the current experimental data for the Al-Zn system.

For the purpose of comparison, this value was also estimated using Eq. (21), as provided in Ref. [23], for the approximate evaluation of $\partial^2 f_{\text{chem}}/\partial c^2$, when undercooling occurs below the critical temperature for coherent spinodal decomposition, taking into account the influence of elastic stress on coherent phase boundaries,

$$\frac{\partial^2 f_{\text{chem}}}{\partial c^2} + \frac{2\eta^2 E}{1-\nu} = 4R(T - T_c)/\Omega, \tag{21}$$

where T_c is the critical temperature for spinodal decomposition. Using the critical temperature of 454 K for the spinodal decomposition of Al-12.5 at.%Zn obtained in Ref. [30], one can obtain a $\partial^2 f_{\text{chem}}/\partial c^2$ value of -5.29×10^9 erg cm^{-3} (shown in Table 8) using Eq. (21).

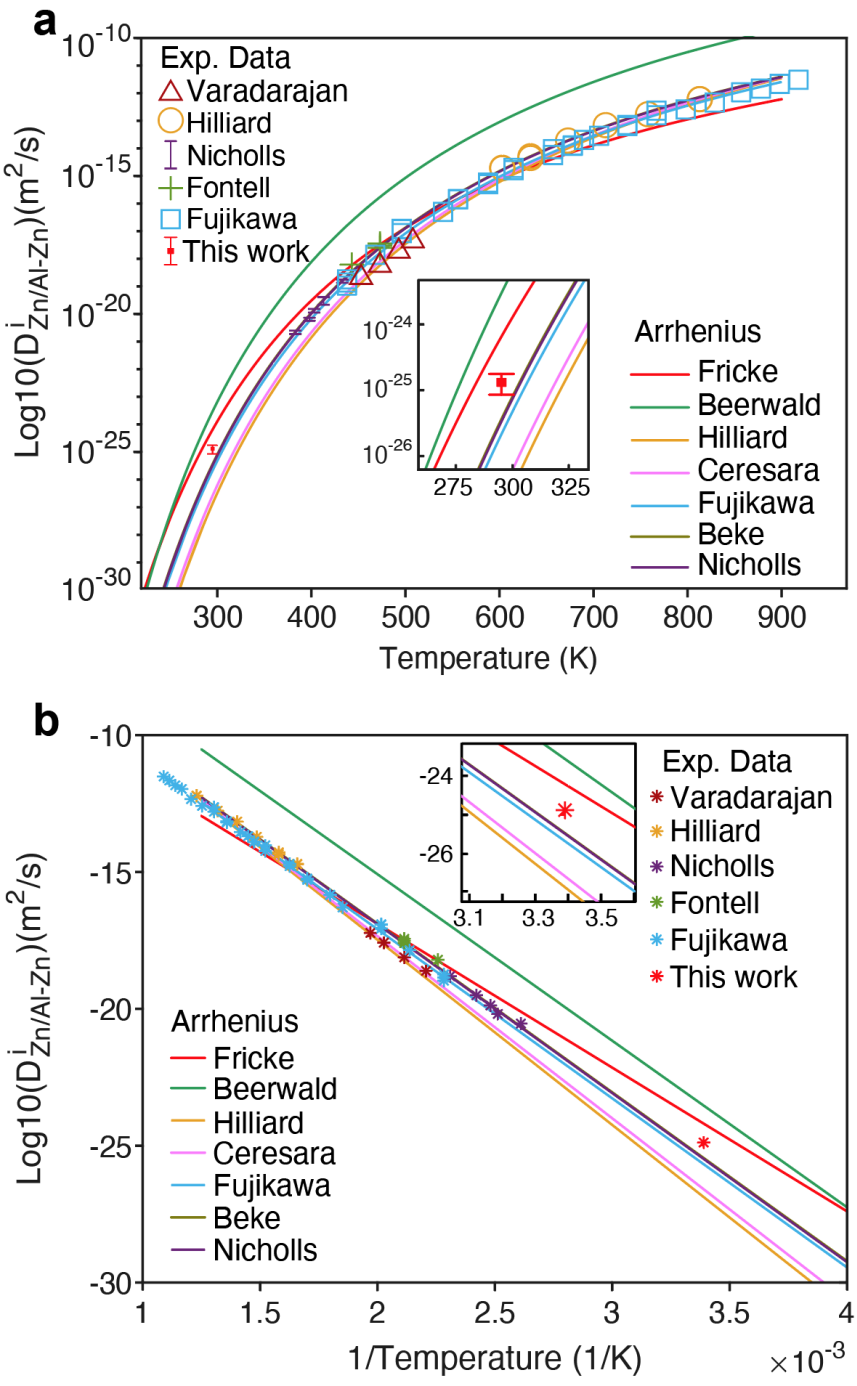

Figure 8: Impurity diffusion coefficients of Zn in Al-Zn solid solution. Refs.: Fontell [38], Nicholls [37], Fujikawa [35], Hilliard [31], Varadarajan [53] Ceresara [34], Beerwald [33], Fricke [32], Beke [36]. a. In normal format. b. Arrhenius plot. Due to data overlap, only a selected part of previous work is shown; a more detailed data summary can be found in [54].

In addition, Rundman and Hilliard [10] provide an estimation equation for $\partial^2 f_{\text{chem}}/\partial c^2$ at $T = T_2$, which does not rely on the critical temperature but rather utilizes an extrapolation of experimentally determined free energies in Al-Zn solid solutions above the miscibility gap ($T = T_1$):

$$\frac{\partial^2 f_{\text{chem}}(T_2)}{\partial c^2} = \frac{RT_2}{\Omega c(1-c)} - 2\left(\frac{f_{\text{Al}}^{\text{E}}}{c^2}\right)_{T_1} - c\frac{\partial}{\partial c}\left(\frac{f_{\text{Al}}^{\text{E}}}{c^2}\right)_{T_1} - (T_2 - T_1)\frac{\partial^2 s^{\text{E}}}{\partial c^2}, \tag{22}$$

where

$$f_{\text{Al}}^{\text{E}} = f_{\text{Al}}^{\text{M}} - RT\ln(1-c)/\Omega, \tag{23}$$

where s^{E} represents the excess integral entropy of mixing per unit volume, and f_{Al}^{M} stands for the partial free energy of mixing per unit volume. Using the parameters at $T_1 = 673$ K from Ref. [55], the calculation yields $\partial^2 f_{\text{chem}}/\partial c^2$ as -9.04×10^9 erg cm^{-3}.

According to Eq. (7), the calculated mobility is approximately inversely proportional to the thermodynamic driving force. Notably, for the values presented in Table 8, variations in the thermodynamic driving force could introduce an error of approximately up to half the magnitude of the measured mobility. Consequently, a precise thermodynamic assessment becomes crucial for enhancing the accuracy of the results.

Table 8: Estimated values of $\partial^2 f_{\text{chem}}/\partial c^2$ (erg cm^{-3}) (c=12.5 at.%) of Al-12.5 at.%Zn at 295 K.

Parameter	Calculated from Eq. (12) [47]	Calculated from Eq. (21) [23]	Calculated from Eq. (22) [10]
$\partial^2 f_{\text{chem}}/\partial c^2$	-6.04×10^9	-5.29×10^9	-9.04×10^9

Other sources of uncertainty in this method include factors such as FIB damage, which can disrupt the initial microstructure and induce defects like dislocations [44], as well as surface diffusion, which leads to a higher diffusion rate near the surface. When applying this method to spinodal decomposition systems, it's essential to exercise caution regarding the limitation on compositional fluctuation wavelength during spinodal decomposition. The suggested critical wavelength should always be significantly smaller than the top radius of the APT specimen.

Despite these factors, this method is applicable for diffusivity measurements ranging from room temperature to artificial aging temperatures, providing valuable insights for designing high-strength aluminum alloys. For instance, the diffusivity value indicates whether the clustering process at room temperature occurs rapidly or slowly under equilibrium vacancy concentrations. This approach can also be used to determine the diffusivity of solutes in other systems that exhibit spinodal decomposition, such as Al-Mg [56, 57], Al-Ag [58], Al-Li [59] and Al-Cu [60].

6. Conclusions

In conclusion, the interdiffusion coefficient of Zn in fcc-Al was determined by analyzing the spinodal decomposition during the nano aging of an Al-12.5 at.%Zn alloy via atom probe tomography and the Cahn-Hilliard theory. At 295 K, the measured interdiffusion coefficient of Zn in the Al-12.5 at.%Zn alloy is $(-2.78 \pm 0.97) \times 10^{-26}$ m^2 s^{-1} and the impurity diffusion coefficient of Zn in the Al-Zn solid solution is $(1.32 \pm 0.46) \times 10^{-25}$ m^2 s^{-1} at 295 K. The method used in this study allows the evaluation of diffusion coefficients within an applicable measurement time at room temperature, compared to traditional methods that measure diffusion length. The nano aging process, which eliminates non-equilibrium vacancies, makes this approach more adaptable to cases where the influence of excess vacancies must be excluded.

Acknowledgements

We acknowledge Prof. John Banhart from the Helmholtz-Centre Berlin for Materials and Energy for his valuable discussion and comments on this work. The original idea came up in the discussion with him on the clustering process in aluminum alloys. Xinren Chen gratefully acknowledges the financial support from the China Scholarship Council (Number: 201806310105). Chuanlai Liu acknowledges financial support from the Deutsche Forschungsgemeinschaft (DFG) within Project C01 of the Collaborative Research Center (SFB) 1394 "Structural and Chemical Atomic Complexity - from defect phase diagrams to material properties", project ID 409476157. Eric Woods acknowledges financial support from the European Research Council (ERC), project ERC-CoG-SHINE-771602. We acknowledge Andreas Sturm for his assistance with the Focused Ion Beam/Scanning Electron Microscopy (FIB/SEM) facilities and Uwe Tezins for his assistance with the Atom Probe Tomography (APT) facilities.

References

[1] J. Banhart, Age Hardening of Aluminum Alloys, in: Heat Treating of Nonferrous Alloys, ASM International, 2016.

[2] K. Shen, Z. Yin, T. Wang, On spinodal decomposition in ageing 7055 aluminum alloys, Materials Science and Engineering: A 477 (2008) 395–398.

[3] D. A. Porter, K. E. Easterling, Phase transformations in metals and alloys (revised reprint), CRC press, 2009.

[4] Z. Yang, I. Erdle, C. Liu, J. Banhart, Clustering and precipitation in Al-Mg-Si alloys during linear heating, Journal of Materials Science & Technology 120 (2022) 78–88.

[5] L. Girifalco, H. Herman, A model for the growth of guinier-preston zones-the vacancy pump, Acta Metallurgica 13 (1965) 583–590.

[6] J. Embury, R. Nicholson, The nucleation of precipitates: the system Al-Zn-Mg, Acta Metallurgica 13 (1965) 403–417.

[7] G. Sha, A. Cerezo, Kinetic monte carlo simulation of clustering in an Al-Zn-Mg-Cu alloy (7050), Acta materialia 53 (2005) 907–917.

[8] H. Löffler, I. Kovacs, J. Lendvai, Decomposition processes in Al-Zn-Mg alloys, Journal of Materials Science 18 (1983) 2215–2240.

[9] G. Dlubek, P. Lademann, H. Krause, S. Krause, R. Unger, Positron lifetime studies of decomposition in 2024 (Al-Cu-Mg) and 7010 (Al-Zn-Cu-Mg) alloys, Scripta materialia 39 (1998) 893–899.

[10] K. Rundman, J. Hilliard, Early stages of spinodal decomposition in an aluminum-zinc alloy, Acta metallurgica 15 (1967) 1025–1033.

[11] R. Acuña, A. Bonfiglioli, Experimental study of random fluctuation effects on spinodal-like decomposition of Al-15 at.% Zn, Acta Metallurgica 22 (1974) 399–408.

[12] J. Silcock, The effect of quenching on the formation of gp zones and θ' in Al Cu-alloys, Philosophical Magazine 4 (1959) 1187–1194.

[13] H. Hagenschulte, T. Heumann, Diffusion, the kirkendall effect and vacancy jump frequency ratios in dilute Al-Zn alloys, Journal of Physics: Condensed Matter 6 (1994) 1985.

[14] A. Kodentsov, A. Paul, Diffusion couple technique: a research tool in materials science, in: Handbook of Solid State Diffusion, Volume 2, Elsevier, 2017, pp. 207–275.

[15] D. C. C. Magalhães, M. F. Hupalo, O. M. Cintho, Natural aging behavior of AA7050 Al alloy after cryogenic rolling, Materials Science and Engineering: A 593 (2014) 1–7.

[16] L. Wan, Y.-L. Deng, L.-Y. Ye, Y. Zhang, The natural ageing effect on pre-ageing kinetics of Al-Zn-Mg alloy, Journal of Alloys and Compounds 776 (2019) 469–474.

[17] Y. Zou, X. Wu, S. Tang, Y. Wang, K. Zhao, L. Cao, The effect of pre-ageing/stretching on the ageing-hardening behavior of Al-Zn-Mg-Cu alloys correlated with Zn/Mg ratio, Materials Science and Engineering: A 830 (2022) 142331.

[18] Y.-S. Lee, D.-H. Koh, H.-W. Kim, Y.-S. Ahn, Improved bake-hardening response of Al-Zn-Mg-Cu alloy through pre-aging treatment, Scripta Materialia 147 (2018) 45–49.

[19] A. Mazilkin, B. Straumal, E. Rabkin, B. Baretzky, S. Enders, S. Protasova, O. Kogtenkova, R. Valiev, Softening of nanostructured Al-Zn and Al-Mg alloys after severe plastic deformation, Acta Materialia 54 (2006) 3933–3939.

[20] Y. Ji, C. Dong, L. Chen, K. Xiao, X. Li, High-throughput computing for screening the potential alloying elements of a 7xxx aluminum alloy for increasing the alloy resistance to stress corrosion cracking, Corrosion Science 183 (2021) 109304.

[21] R. Swalin, Correlation between frequency factor and activation energy for solute diffusion, Journal of Applied Physics 27 (1956) 554–555.

[22] C. Zener, Theory of do for atomic diffusion in metals, Journal of Applied Physics 22 (1951) 372–375.

[23] J. W. Cahn, On spinodal decomposition, Acta metallurgica 9 (1961) 795–801.

[24] H. Cook, Brownian motion in spinodal decomposition, Acta metallurgica 18 (1970) 297–306.

[25] J. Hoyt, B. Clark, D. De Fontaine, J. Simon, O. Lyon, A synchrotron radiation study of phase separation in Al-Zn alloys—I. kinetics, Acta Metallurgica 37 (1989) 1597–1609.

[26] B. Gault, A. Chiaramonti, O. Cojocaru-Mirédin, P. Stender, R. Dubosq, C. Freysoldt, S. K. Makineni, T. Li, M. Moody, J. M. Cairney, Atom probe tomography, Nature Reviews Methods Primers 1 (2021) 51.

[27] J. Zhou, J. Odqvist, M. Thuvander, P. Hedström, Quantitative evaluation of spinodal decomposition in Fe-Cr by atom probe tomography and radial distribution function analysis, Microscopy and Microanalysis 19 (2013) 665–675.

[28] P. Dumitraschkewitz, P. J. Uggowitzer, S. S. Gerstl, J. F. Löffler, S. Pogatscher, Size-dependent diffusion controls natural aging in aluminium alloys, Nature communications 10 (2019) 1–6.

[29] J. Banhart, Y.-S. Chen, Q. Guo, R. Marceau, J. Cairney, Direct ageing experiments on nanometre-scale aluminium alloy samples, Acta Materialia 231 (2022) 117848.

[30] T. Ungár, J. Lendvai, I. Kovács, Determination of the spinodal temperature in a series of Al-Zn (6–21 at.%) alloys, Philosophical Magazine A 43 (1981) 927–934.

[31] J. Hilliard, B. Averbach, M. Cohen, Self and interdiffusion in aluminum-zinc alloys, Acta Metallurgica 7 (1959) 86–92.

[32] W. Fricke, K.R. van Horn, Aluminum, Properties, Physical Metallurgy and Phase Diagrams, American Society for Metals, Metals Park, OH, volume 1, American Society for Metals, Metals Park, OH, 1967.

[33] A. Beerwald, Diffusion of various metals in aluminum, Z Elektrochem Angew Phys Chem 45 (1939) 789–795.

[34] S. Ceresara, T. Federighi, F. Pieragostini, Determination of diffusion coefficients in metals by a resistometric method-application to the diffusion of Zn in Al, physica status solidi (b) 16 (1966) 439–447.

[35] S. Fujikawa, K.-i. Hirano, Diffusion of 65Zn in aluminum and Al-Zn-Mg alloy over a wide range of temperature, Transactions of the Japan Institute of Metals 17 (1976) 809–818.

[36] D. Beke, I. Gödeny, F. Kedves, G. Groma, Diffusion of 65Zn in dilute AlZn, AlMg, AlZnMg and AlZnFe alloys, Acta Metallurgica 25 (1977) 539–550.

[37] A. Nicholls, I. Jones, Determination of low temperature volume diffusion coefficients in an Al-Zn alloy, Journal of Physics and Chemistry of Solids 44 (1983) 671–676.

[38] A. Fontell, E. Arminen, M. Turunen, Application of the backscattering method for the measurement of diffusion of zinc in aluminium, physica status solidi (a) 15 (1973) 113–119.

[39] Y. Cui, K. Oikawa, R. Kainuma, K. Ishida, Study of diffusion mobility of Al-Zn solid solution, Journal of phase equilibria and diffusion 27 (2006) 333–342.

[40] B. Gault, M. P. Moody, F. De Geuser, G. Tsafnat, A. La Fontaine, L. T. Stephenson, D. Haley, S. P. Ringer, Advances in the calibration of atom probe tomographic reconstruction, Journal of Applied Physics 105 (2009) 034913.

[41] S. Agarwal, H. Herman, Spinodal decomposition in liquid-quenched Al-22 at .% Zn, Scripta Metallurgica 7 (1973) 503–508.

[42] M. Miller, E. Kenik, Atom probe tomography: A technique for nanoscale characterization, Microscopy and Microanalysis 10 (2004) 336–341.

[43] F. De Geuser, W. Lefebvre, D. Blavette, 3D atom probe study of solute atoms clustering during natural ageing and pre-ageing of an Al-Mg-Si alloy, Philosophical Magazine Letters 86 (2006) 227–234.

[44] B. Gault, M. P. Moody, J. M. Cairney, S. P. Ringer, Atom probe microscopy, volume 160, Springer Science & Business Media, 2012.

[45] L.-Q. Chen, Phase-field models for microstructure evolution, Annual review of materials research 32 (2002) 113–140.

[46] S. B. Biner, et al., Programming phase-field modeling, Springer, 2017.

[47] A. Dinsdale, O. Zobac, A. Kroupa, A. Khvan, Use of third generation data for the elements to model the thermodynamics of binary alloy systems: Part 1–the critical assessment of data for the Al-Zn system, Calphad 68 (2020) 101723.

[48] M. Hillert, Partial gibbs energies from Redlich-Kister polynomials, Thermochimica acta 129 (1988) 71–75.

[49] J. W. Cahn, J. E. Hilliard, Free energy of a nonuniform system. i. interfacial free energy, The Journal of chemical physics 28 (1958) 258–267.

[50] E. Huston, J. W. Cahn, J. Hilliard, Spinodal decomposition during continuous cooling, Acta metallurgica 14 (1966) 1053–1062.

[51] L. S. Darken, Diffusion, mobility and their interrelation through free energy in binary metallic systems, Trans. Aime 175 (1948) 184–201.

[52] H. Mehrer, 1.4 The various diffusion coefficients: Diffusion in Solid Metals and Alloys, Springer Materials, volume 36, Springer-Verlag Berlin Heidelberg, 1990.

[53] S. Varadarajan, R. Fournelle, Low temperature volume diffusion of zinc in aluminium, Acta metallurgica et materialia 40 (1992) 1847–1854.

[54] Y. Du, Y. Chang, B. Huang, W. Gong, Z. Jin, H. Xu, Z. Yuan, Y. Liu, Y. He, F.-Y. Xie, Diffusion coefficients of some solutes in fcc and liquid Al: critical evaluation and correlation, Materials Science and Engineering: A 363 (2003) 140–151.

[55] J. Hilliard, B. Averbach, M. Cohen, Thermodynamic properties of solid aluminum-zinc alloys, Acta Metallurgica 2 (1954) 621–631.

[56] Y. Tang, W. Goto, S. Hirosawa, Z. Horita, S. Lee, K. Matsuda, D. Terada, Concurrent strengthening of ultrafine-grained age-hardenable Al-Mg alloy by means of high-pressure torsion and spinodal decomposition, Acta Materialia 131 (2017) 57–64.

[57] W. Zhong, M. S. Hooshmand, M. Ghazisaeidi, W. Windl, J.-C. Zhao, An integrated experimental and computational study of diffusion and atomic mobility of the aluminum–magnesium system, Acta Materialia 189 (2020) 214–231.

[58] K. Moore, W. Johnson, J. Howe, H. Aaronson, D. Veblen, On the interaction between Ag-depleted zones surrounding γ plates and spinodal decomposition in an Al-22 at.% Ag alloy, Acta materialia 50 (2002) 943–956.

[59] V. Radmilovic, A. Fox, G. Thomas, Spinodal decomposition of Al-rich Al-Li alloys, Acta Metallurgica 37 (1989) 2385–2394.

[60] L. Löchte, A. Gitt, G. Gottstein, I. Hurtado, Simulation of the evolution of GP zones in Al–Cu alloys: an extended Cahn–Hilliard approach, Acta materialia 48 (2000) 2969–2984.